Materials Research. 2023; 26:e20230278
DOI: https://doi.org/10.1590/1980-5373-MR-2023-0278

Improving the Wear Resistance of High Chromium Cast Iron through High Entropy Alloys Concepts and Microstructure Refinement

Willian Martins Pasini[b], Leonardo Pereira[a], Adam Bitka[b], Konrad Chrzan[b], Waclaw Oleksy[b], Krzysztof Jaśkowiec[b], Tomasz Polczyk[b], Wojciech Polkowski[b], Tomasz Dudziak[b], Carlos Alexandre dos Santos[c], Vinicius Karlinski de Barcellos[a]*

[a]Universidade Federal do Rio Grande do Sul (UFRGS), Programa de Pós-Graduação em Engenharia de Minas, Metalúrgica e de Materiais (PPGE3M), 91501-970, Porto Alegre, RS, Brasil.
[b]Łukasiewicz Research Network, Krakow Institute of Technology (KIT), Krakow, Poland.
[c]Pontifícia Universidade Católica do Rio Grande do Sul (PUCRS), Programa de Pós-Graduação em Engenharia e Tecnologia de Materiais (PGETEMA), 90619-900, Porto Alegre, RS, Brasil.

Received: June 16, 2023; Revised: September 06, 2023; Accepted: October 31, 2023.

High Chromium Cast Iron (HCCI) has demonstrated its effectiveness as a potential material for applications in severe environments due to its remarkable wear resistance attributed to the volumetric fraction of carbides in the microstructure. This study investigates a novel high-alloyed composition of white cast iron named High Entropy White Cast Iron (HEWCI), which merges the concepts of HCCI and high entropy alloys. Specifically designed chemical compositions incorporating Vanadium (V), Molybdenum (Mo), and Nickel (Ni) were employed to enhance its wear resistance properties. The solidification path, microstructural characterization, and wear responses of HEWCI were evaluated. XRD and SEM techniques were carried out for characterization purposes. Linearly reciprocating ball-on-flat sliding wear tests were conducted using a high-frequency reciprocation rig (HFRR) tribometer, assessing wear volume, linear wear rate, specific wear rate (κ), and coefficient of friction (COF). The results revealed microstructural refinement and precipitation of new carbides through V, Ni, and Mo additions. This approach demonstrates that adding carbide-forming elements and refining the microstructure are promising strategies for enhancing wear performance in HEWCI alloys.

Keywords: *high entropy alloys, high chromium cast irons, solidification, microstructures, wear resistance.*

1. Introduction

White cast irons (WCIs) have been extensively utilized in many industries requiring wear resistance[1-3]. WCIs for wear resistance proposes are typically classified into four groups: pearlitic, Ni-Hard (with M_3C eutectic carbides or M_7C_3 eutectic carbides), High-Chromium Cast Iron (HCCI), and Multi-Component Cast Iron (MCCI)[4-6].

Among these, Ni-Hard and HCCI are the most commonly utilized commercial alloys in industrial applications that require wear resistance. Ni-Hard refers to a group of white cast irons alloyed with Ni and Cr, with exceptional hardness and remarkable abrasion resistance. In scenarios where toughness, abrasion resistance, and, in some cases, corrosion resistance are considered, the HCCI stands unrivaled. Within the Ni-Hard family, Ni-Hard 4 exhibits the highest Ni, Cr, and Si levels. On the other hand, the HCCI family can have Cr content that is 2 to 3 times higher than that of Ni-Hard 4. Despite these differing chemical compositions, both alloys exhibit similar microstructures characterized by M_7C_3 eutectic carbides[4,5].

MCCI contains Cr and other alloying elements that tend to form new carbides, such as Ti, V, Nb, Mo, and W. The carbon content of MCCI ranges between the carbon values of High-Speed Tool Steel, Ni-Hard, and HCCI. During solidification, carbides such as MC and M_2C precipitate in the microstructure of these alloys. MCCI demonstrates superior resistance to abrasive wear after heat treatment, compared to HCCI, even with a lower volume fraction of carbides[6,7].

The "base element approach" has been used in metallurgical history to develop metallic alloys. This method uses one primary element as the matrix and additional elements to improve properties. Recently, there has been a growing interest in developing a novel alloy design approach inspired by new systems that combine five or more elements. This approach created "High Entropy Alloys" (HEAs)[8].

This concept has greatly expanded alloy design and allowed the exploration of new alloy systems. HEAs were initially defined as alloys with at least five primary alloying elements in amounts ranging from 5 to 35 atomic percent, and these alloys have single-phase solid solution structures and configurational entropy (ΔS_{conf}) greater than 12.5 kJ/mol (1.5R, where R is the gas constant)[8-11].

However, as initially proposed, the strict definition of HEAs limited studies to alloys containing five or more principal elements and only single-phase solid-solutions microstructures.

*e-mail: vinicius.karlinski@ufrgs.br

Recognizing the complexities associated with attempting to fully define HEAs based on a single definition and microstructure new terminologies were introduced to overcome these limitations. These new terminologies include Complex Concentrated alloys (CCAs) and entropy-enhanced Conventional Alloys (EECAs) to encompass a broader range of alloy chemical compositions and microstructures[11].

Building upon the concepts of WCIs and HEAs, Wang et al.[12,13] modified the chemical compositions of high-Cr cast irons by adding mixtures of various carbide-forming elements. They noticed that these tailored HCCIs showed high sliding wear resistance. The type, shape, phase fraction, and distribution of hard carbides in the microstructure, as well as the properties of the supporting matrix, significantly impact wear performance. It is well recognized that incorporating carbide-forming elements such as Mo, W, V, and Nb into the alloy can enhance wear resistance. Developing new abrasion-resistant cast iron based on a multi-component approach is a well-known research topic, with many studies supporting this hypothesis. Different high-alloyed cast iron compositions have been studied by diverse researchers such as Matsubara et al.[14], Kusumoto et al.[6], Purba et al.[15], Pasini et al.[16] and Bedolla-Jacuinde et al.[17]. The influence of Ni on the multi-component cast iron has also been studied by Kusumoto et al.[7].

This study explores High Entropy White Cast Iron (HEWCI), establishing a bridge between the metallurgy of white cast iron and high entropy alloy concepts. In this work, three different chemical compositions were proposed and selected to investigate solidification, mechanical properties, and sliding wear behavior.

2. Materials and Methods

2.1. Alloys Design

Modifications were made to a hypoeutectic High-Chromium Cast Iron (HCCI) alloy, considered the base alloy, to design the High Entropy White Cast Iron (HEWCI) alloys. The selected alloying elements for this purpose were V, Mo, and Ni, commonly employed in the metallurgy of steel and cast iron and have well-known effects on microstructures. Nickel was chosen because it aids in forming eutectic M_7C_3 carbides with Cr and is required to produce a pearlite-free matrix structure. On the other hand, the V and Mo additions are due to a strong tendency to form hard carbides, elements widely used in the metallurgy of tool steels and high-speed steels. Adding high amounts of these elements to HEWCI alloys aims to improve the hardening ability.

During the design process, the following definitions of high entropy alloys were considered as design boundaries: (i) alloy containing at least five major elements; (ii) at least five percent concentration of each element; and (iii) having configurational entropy of mixing, $\Delta S_{mix} \geq 1.5$ R in the random-solution state. The chemical compositions of the HEWCI alloys were determined using optical emission spectrometry (MiniLab 300, GNR Analytical Instruments), and the obtained chemical compositions can be found in Table 1. As observed, the design criteria considered for high entropy alloys were achieved.

2.2. Alloys preparation and thermal analysis

To produce the HEWCI alloys, pure Ni and C, Fe-Si, Fe-Mn, Fe-V, and Fe-Mo master alloys were added to the hypoeutectic High Chromium Cast Iron (HCCI) base alloy. The HEWCI alloys were melted in a 4 kg coreless induction furnace. The metal was heated at 1400°C, and after removing any slag, the resulting molten alloys were poured into a cylindrical permanent copper mold to obtain samples for mechanical tests and a thermal-analysis samples cup. Approximately 700 g of each molten alloy was poured into two shell-molding sand cups instrumented with type-K thermocouples to analyze the solidification sequence of each new cast iron under near-equilibrium conditions. Computer-Aided Cooling Curve Analysis (CCA-CA) was performed during the solidification to reveal all the solid-liquid reactions and to determine the solidification path of the HEWCI alloys.

2.3. Microstructure characterization

For microstructure analysis, the HEWCIs were cut from the shell-molding sand thermal analysis cups near the type-K thermocouple and prepared by grinding with SiC papers ranging from 240 to 1200 grit, followed by fine polishing with alumina suspension. Scanning electron microscopy (SEM), utilizing backscattered electron (BSE) and secondary electron (SE) imaging modes associated with energy-dispersive X-ray spectroscopy (EDS), was used to characterize the matrix and carbides. X-ray diffraction (XRD, CuKα1 radiation, 40 kV, 30 mA, 2θ:20–100) analyses using powders obtained from each alloy were performed to identify the type and chemical composition of the phases.

2.4. Mechanical properties

The ultimate tensile strength (UTS) responses of the HCCI, HEWCI-A, HEWCI-B, and HEWCI-C alloys were investigated through room-temperature monotonic tensile testing.

Table 1. Chemical compositions of the hypoeutectic cast irons (at. %).

	C	Mn	Si	Cr	Mo	V	Ni	ΔS_{mix}
HCCI	2.47	1.67	1.37	18.90	0.02	0.11	0.12	0.96 R
HEWCI-A	2.31	1.51	1.27	18.49	6.32	4.05	10.38	1.50 R
HEWCI-B	2.33	1.71	1.41	18.62	12.78	3.56	4.76	1.50 R
HEWCI-C	2.39	2.67	1.41	18.47	11.60	5.96	9.62	1.65 R

Non-standard, bone-shaped specimens were machined using electrical discharge machining (EDM) from as-cast HEWCI cylindrical specimens obtained from the permanent copper mold, following the geometry indicated in Figure 1a. The tensile tests conducted at a constant strain rate ($6.4x10^{-3}s^{-1}$) were performed using a Zwick Roell AllroundLine Z10 machine equipped with a 10 kN load cell and a dedicated specimen grip. The laserXtens HP1-15 high precision (0.5 class) speckle-type laser extensometer was used in conjunction with optical cameras for non-contact strain measurements. The ultimate tensile strength (UTS) was automatically extracted from the recorded curves using the ZwickRoell testXpert II software. Figure 1b illustrates the experimental setup that was employed.

2.5. Wear tests

The sliding wear performance of the HEWCIs was evaluated through reciprocating sliding wear testing using a high-frequency reciprocating rig (Ducom, HFRR 4.2), following the guidelines of the ASTM G133 standard test method[18]. In this setup, a sphere (counter-body) undergoes linear and reciprocating movement against the surface of the material (disc) being analyzed. The dry reciprocating sliding tests were conducted at room temperature. An alumina ball (Ø = 6 mm, 74/80 HRC hardness) was used as the counterpart. The stroke distance was 1 mm, the reciprocating frequency was 50 Hz, and a 2N load was applied. The as-cast HEWCI specimens, which were machined using EDM from copper-mold ingots, ground using abrasive papers with grit sizes of #220, 320, 400, 600, and 1200, followed by sequential polishing using alumina suspension with particle sizes of 1 µm and 0.3 µm. During the tests, frictional force data were collected and subsequently used to calculate the coefficient of friction (COF or μ_C). The wear volumes (V) and profiles of the HEWCI samples were determined according to the ASTM D7755 standard[19], and the linear wear rate (W_l) and specific wear rate (κ) were calculated.

3. Results and Discussion

3.1. Solidification and thermal analysis

Considering that the HEWCI alloys consist of multiple components with significant carbide-forming abilities and the need for well-established phase diagrams for such multi-component systems in the literature, accurately estimating all stages of solidification solely based on the as-cast structure is challenging. In order to gain further insights into the solidification path of the HCCI, HEWCI-A, HEWCI-B, and HEWCI-C alloys, X-ray diffraction (XRD), backscattered electron (BSE) images and Newtonian thermal analyses were conducted. Figure 2 illustrates the results of phase identification for the as-cast alloys obtained from XRD spectra (Figure 2a) and BSE images (Figure 2b). The XRD analyses revealed the presence of austenite (γ), M_2C carbides (Mo_2C and V_2C), M_7C_3 carbide, and M_6C carbide in the alloys.

The Newtonian analysis method, utilizing the first derivative of the cooling curve, was employed to determine the temperatures at which phase transitions occurred during the cooling of the alloys. Additionally, the first derivative of the cooling curve was compared to the Zero Curve, which represents the cooling rate of the alloy without any phase transformations, to gain further insights. This methodology allows the identification of peaks and inflections in the cooling rate curves corresponding to phase transformations, which are influenced by the heat transfer between the latent heat released during solidification and the heat dissipated to the environment[20].

The cooling curve of the HCCI alloy, as shown in Figure 3a, exhibits three distinct reaction or arrest points labeled as R1, R3, and T_{sol}, occurring at temperatures of 1324°C, 1247°C, and 1233°C, respectively. The identification of the solidification reactions at each arrest point was conducted by examining the final microstructure of the alloy and comparing it to the findings of previous studies on the Fe-Cr-C system carried out by Thorpe and Chicco[21]. The first arrest point (R1) on the

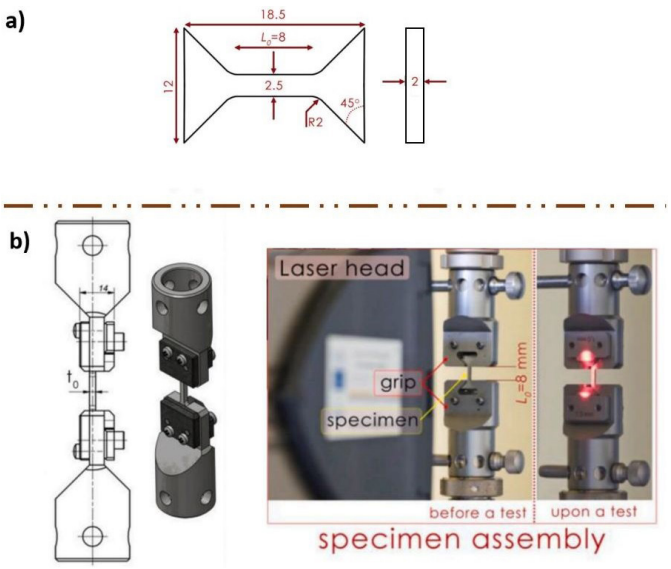

Figure 1. (a) Configuration of the non-standard specimen for tensile tests, (b)Drawing of the applied sample grip and a macro view of the experimental setup comprising a 10 kN tensile machine and a non-contact speckle-type laser extensometer.

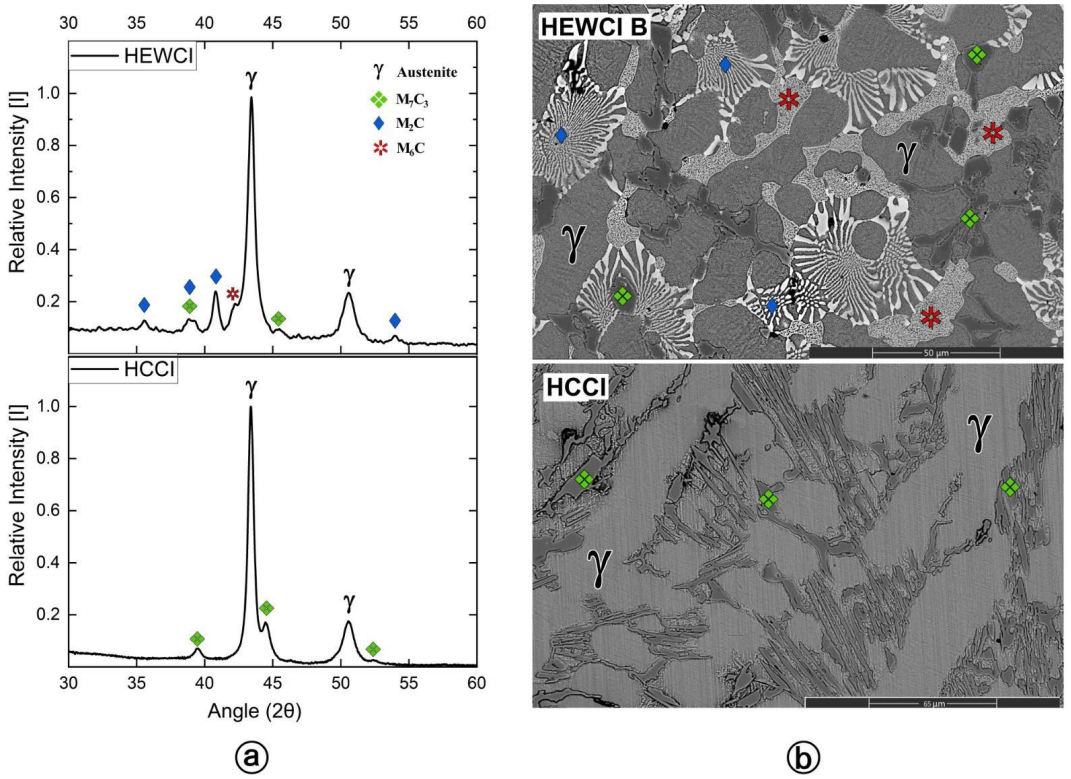

Figure 2. (a) Identification of austenite, M_2C, M_7C_3, and M_6C phases by XRD diffraction analyses, and (b) BSE images of the as-cast microstructures of HEWCI-B and HCCI alloys.

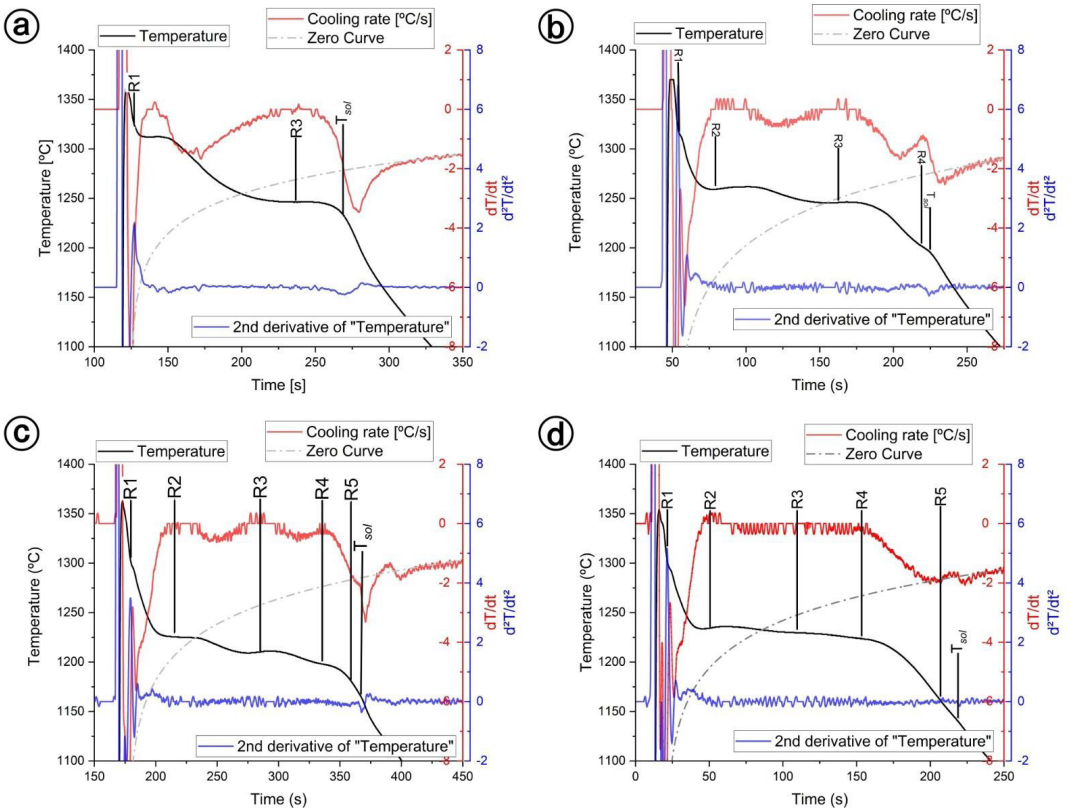

Figure 3. The cooling curves, zero curve, 1st and 2nd derivative: a) HCCI, b) HEWCI-A, c) HEWCI-B, d) HEWCI-C.

cooling curve (Figure 3a) corresponds to the formation of primary γ-austenite. The second arrest point (R3) represents the transformation of liquid to the eutectic mixture of γ and M_7C_3 carbides. The T_{sol} point indicates the minimum value of the second derivative of the cooling curve, corresponding to the end of solidification or the cross-point between the first derivative and the Zero Curve.

The XRD diffractograms of the HEWCI-A, HEWCI-B, and HEWCI-C alloys exhibited similar patterns, indicating the presence of almost identical indexed carbide phases. The solidification sequence of these alloys involved the formation of primary γ-austenite (R1), M_2C (V-rich) carbide (R2), M_7C_3 (Cr-rich) carbide (R3), and M_2C (Mo-rich) carbide (R4). The cooling curves for HEWCI alloys are presented in Figures 3b-d. In the case of HEWCI-B and HEWCI-C, the curves showed an additional peak on the first derivative curve, labeled as R5 in Figure 3c and Figure 3d. Based on this observation and the identification of M_6C carbide through XRD analyses in the HEWCI-B and HEWCI-C alloys, it can be inferred that M_6C is formed as the final phase transformation during solidification. The temperatures of the arrest reactions are summarized in Table 2.

3.2. Microstructure characterization

Microstructure observations obtained by SEM in BSE mode indicate the presence of five constituent phases, which have been indexed by XRD and are shown in Figure 4. These phases include (a) M_2C carbides (light gray), (b) M_7C_3 carbides (dark gray), (c) M_2C carbides (white), and (d) M_6C carbides (fuzzy gray). The M_2C (V-rich) carbides are primarily within the Solidification Cell (SC). In contrast, the M_7C_3 (Cr-rich), M_2C (Mo-rich), and M_6C (Mo, Fe-rich) carbides are distributed along the Cell Boundaries (CB) following the solidification direction.

In Figure 5, a micrograph of HEWCI reveals the presence of different carbides, indicated by the letters “a” through “d”, where EDS analyses were conducted, and the corresponding results are presented in Figures 5a-d. The region marked by the letter (a) exhibits the highest concentration of V, indicating the presence of an M_2C (high-V) carbide (Figure 5a). The dark-gray region marked by the letter (b) corresponds to an M_7C_3 carbide, primarily composed of Cr (Figure 5b). The white-colored region marked by the letter (c) shows a higher Mo content compared to other carbide-forming elements, identifying it as an M_2C (high-Mo) carbide with a lamellar morphology (Figure 5c). The areas marked by the letter (d) are identified as an M_6C carbide, consisting predominantly of Fe and Mo elements (Figure 5d).

The HEWCI alloy has multiple elements that exhibit a pronounced tendency to form carbides. Figure 6 illustrates the distribution of chemical elements, revealing the partial solubility of carbide-forming elements within one or more carbides across different alloy regions. Mo demonstrates partial solubility in V-rich carbides, forming M_2C (Mo-rich) carbides at the boundaries of the M_2C (V-rich) phase. The remaining liquid phase precipitates as M_6C carbides with relatively lower V content. As mentioned, the carbides observed in the HEWCI alloys are multi-component and enriched with V, Cr, and Mo, as these elements exhibit a stronger affinity for carbon than iron.

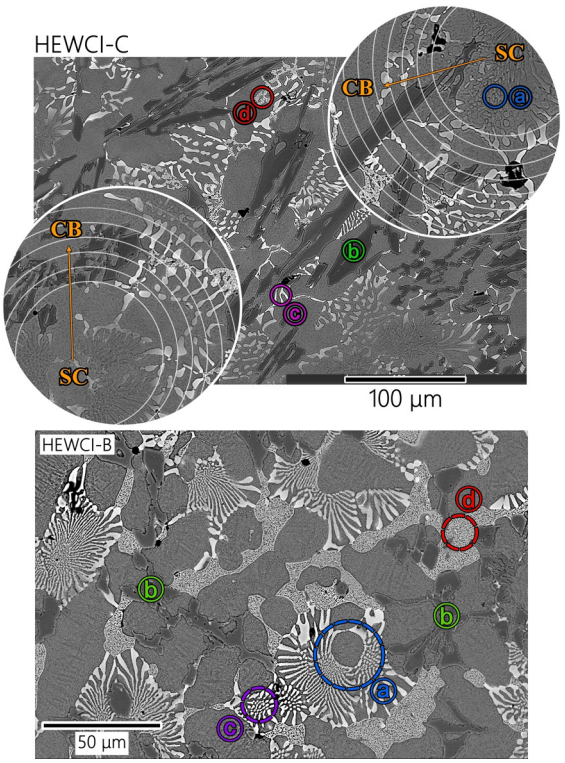

Figure 4. Backscattered electron (BSE) images of the microstructures of as-cast HEWCI-B and HEWCI-C alloys obtained from thermal analysis. (a) M_2C (V-rich), (b) M_7C_3 (Cr-rich), (c) M_2C (Mo-rich), and (d) M_6C (Mo, Fe-rich) carbides.

Table 2. Estimated solidification sequence for the HCCI and HEWCI alloys.

Solidification sequence	Alloy	Temperatures (ºC)					
R1: $L_A \rightarrow \gamma + L_B$		R1	R2	R3	R4	R5	T_{sol}
R2: $\gamma + M_2C$(V-rich)$+ L_C$	HCCI	1324	-	1246	-	-	1231
R3: $\gamma + M_7C_3 + L_D$	HEWCI-A	1319	1259	1246	1202	-	1195
R4: $\gamma + M_2C$ (Mo-rich)$+L_E$	HEWCI-B	1305	1225	1210	1198	1182	1164
R5: $\gamma + M_6C$ (Mo-rich)	HEWCI-C	1303	1234	1229	1223	1161	1140

$L_{A\text{-}E}$ are solute-rich liquid phases.

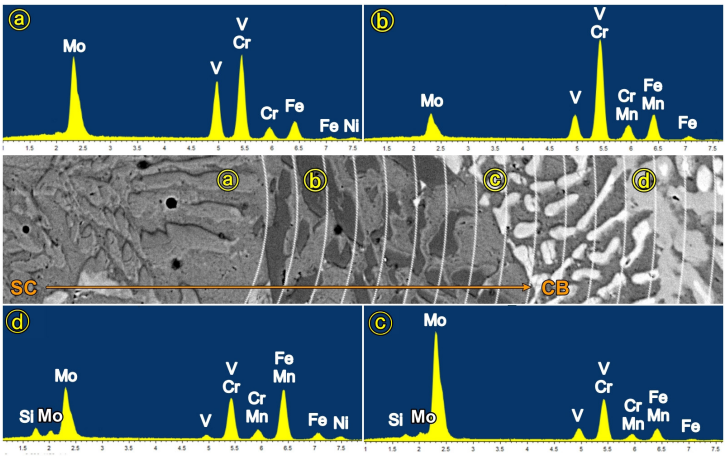

Figure 5. SEM micrograph of HEWCI-C, with corresponding EDS spectra for areas marked (a) through (d).

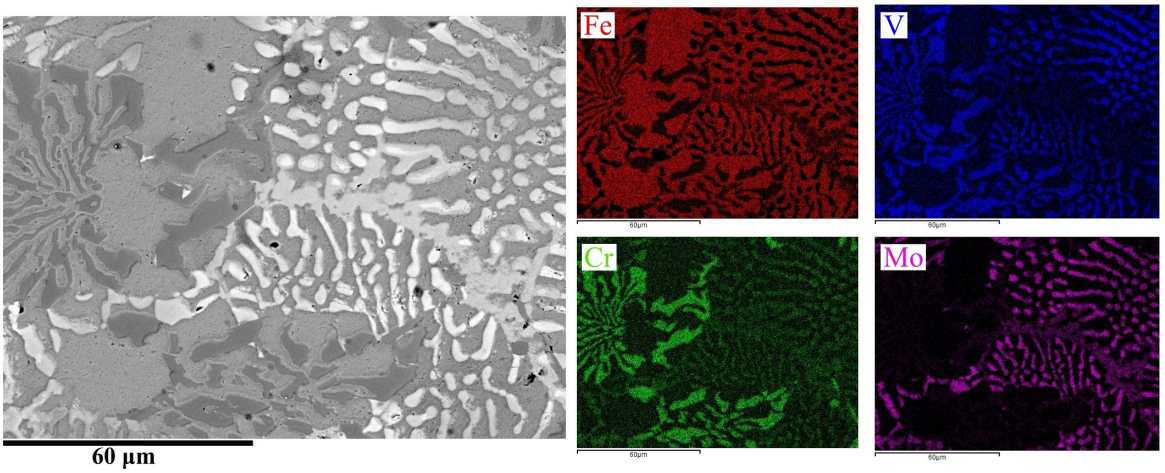

Figure 6. EDS mapping of the chemical composition of HEWCI-C, demonstrating the partial solubility of the carbide-forming elements in different carbides within the HEWCI.

3.3. Mechanical properties and sliding wear behavior

The ultimate tensile strength and strain-to-fracture results of the HEWCI alloys are presented in Table 3. The alloying element additions resulted in an improvement in both tensile strength and strain values. This can be attributed to the microstructural refinement achieved in the HEWCI alloys, the formation of new second-phase precipitates, and the solid solution strengthening. The microstructural refinement can be observed in Figure 7, where a comparison is made between HCCI and HEWCI alloys. These findings agree with previous studies by Hashimoto et al.[22-25], supporting the notion that the influences of elements V, Mo, and Ni significantly enhance the mechanical properties of HEWCI alloys.

The ASTM G133 standard[18] describes a method for evaluating material wear through a linearly reciprocating ball-on-flat sliding wear test. The results are summarized in Table 3. The wear tracks were characterized using three-dimensional optical profilometry (Bruker 3D Optical Profilometer - GTK M, CONTOUR GTK). A three-dimensional surface profile was generated for each track, allowing for the measurement of the wear volume and the acquisition of the central profile, track depth, and width, as illustrated in Figure 8.

Figure 8a presents the wear volume (V) and specific wear rate (κ) of the alloys, while Figure 8b compares the cross-section profiles of the wear tracks between the HEWCI and HCCI alloys after the tests. It is observed in Table 3 and Figure 8 that the high-entropy alloys with added V, Mo, and Ni exhibited improved wear resistance. The specific wear rate decreases for all HEWCI alloys as the content of alloying elements increases. The HEWCI-A alloy has a specific wear rate that is 48% lower than that of the base HCCI alloy, while the HEWCI-B alloy has a wear rate that is 37% lower than HCCI. In terms of wear resistance, the HEWCI-C alloy exhibits similar behavior to the HEWCI-A alloy. The coefficients of friction were measured during the sliding wear tests. Initially, the coefficient of friction increased rapidly, and after a 10m sliding distance, it reached a steady-state regime. According to Table 3, the COFs of the HEWCI alloys in the investigated conditions ranged from 0.27 to 0.33. No evident differences in the COFs among the alloys were observed.

Table 3. Tensile strength (σ_{UTS}), strain-to-fracture, coefficient of friction (COF), wear volume (V), and specific wear rate (κ) of HCCI and HEWCI alloys.

Alloy	σ_{UTS} (MPa)	Strain-to-Fracture (%)	COF	V (mm^3)	κ (mm^3/Nm)
HCCI	571	0.21	0.302	0.0026	1.87 E-8
HEWCI A	657	0.62	0.276	0.0013	0.98 E-8
HEWCI B	854	0.88	0.324	0.0015	1.16 E-8
HEWCI C	795	0.70	0.293	0.0014	0.95 E-8

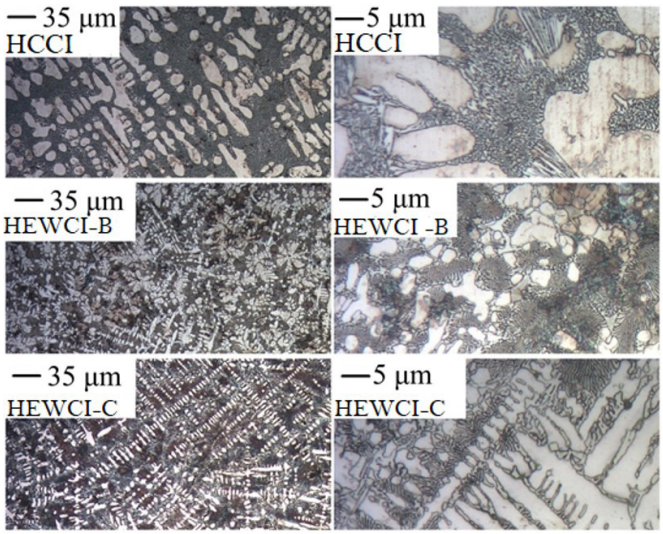

Figure 7. Comparison of microstructural refinement between HEWCI alloys and HCCI alloys.

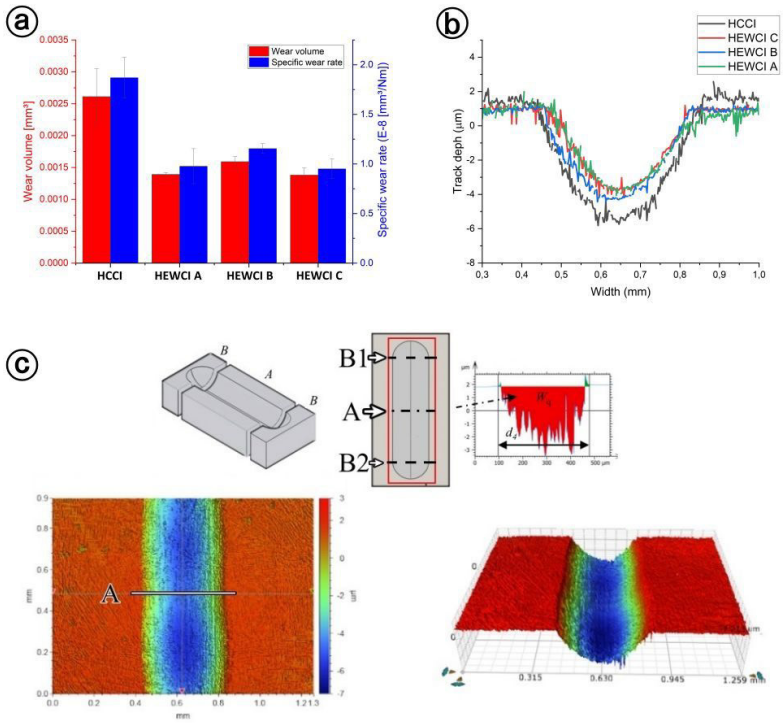

Figure 8. (a) Wear volume and specific wear rate of the HEWCI alloys, (b) Cross-section profiles of the wear track, and (c) Three-dimensional profilometry image used for the calculation of wear volume.

4. Conclusion

New abrasion-resistant white cast iron alloys were developed, combining the concepts of high entropy alloys with the conventional metallurgy of high chromium cast iron (HCCI). Three modified alloys were successfully produced, containing more than five alloying elements and exhibiting a configuration entropy greater than 1.5R. The base hypoeutectic (HCCI) alloy was enhanced by adding carbide-forming elements such as V, Mo, and the non-carbide-forming element Ni. The incorporation of these carbide-forming elements resulted in the refinement of M_7C_3 eutectic carbides and the formation of new, finer carbides, including M_2C and M_6C.

The high-entropy wear-resistant cast irons (HEWCI) exhibited improved resistance to wear and mechanical properties, which can be attributed to its refined microstructure and the presence of various types of fine carbides, including M_2C (V-rich), M_2C (Mo-rich), M_6C, and M_7C_3. The addition of alloying elements led to an average increase in tensile strength of 34.5%. Notably, the average strain to fracture in HEWCI showed a significant improvement, increasing by approximately 3.5 times compared to HCCI. Regarding the specific wear rate, HEWCI demonstrated an average response of approximately 40% better than the base alloy.

5. Acknowledgments

The authors acknowledge the Brazilian research agencies CNPq, CAPES, and FINEP for financial support.

6. References

1. Çöl M, Koç FG, Öktem H, Kır D. The role of boron content in high alloy white cast iron (Ni-Hard 4) on microstructure, mechanical properties and wear resistance. Wear. 2016;348-349:158-65.
2. Doğan ÖN, Hawk JA, Laird G 2nd. Solidification structure and abrasion resistance of high chromium white irons. Metall Mater Trans, A Phys Metall Mater Sci. 1997;28(6):1315-28.
3. Adler TA, Doğan ÖN. Erosive wear and impact damage of high-chromium white cast irons. Wear. 1999;225-229:174-80.
4. Jokari-Sheshdeh M, Ali Y, Gallo SC, Lin W, Gates JD. Comparing the abrasion performance of NiHard-4 and high-Cr-Mo white cast irons: the effects of chemical composition and microstructure. Wear. 2022;492-493:204208.
5. Laird G, Gundlach R, Röhrig K. Abrasion-resistant cast iron handbook. Materials Park: ASM; 2000.
6. Kusumoto K, Shimizu K, Yaer X, Zhang Y, Ota Y, Ito J. Abrasive wear characteristics of Fe-2C-5Cr-5Mo-5W-5Nb multi-component white cast iron. Wear. 2017;376-377:22-9.
7. Kusumoto K, Shimizu K, Efremenko VG, Hara H, Shirai M, Ito J, et al. Three body type abrasive wear characteristics of multi-component white cast irons. Wear. 2019;426-427:122-7.
8. Yeh J-W, Chen S-K, Lin S-J, Gan J-Y, Chin T-S, Shun T-T, et al. Nanostructured High-entropy alloys with multiple principal elements: novel alloy design concepts and outcomes. Adv Eng Mater. 2004;6(5):299-303.
9. Zhang Y, Zuo TT, Tang Z, Gao MC, Dahmen KA, Liaw PK, et al. Microstructures and properties of high-entropy alloys. Prog Mater Sci. 2014;61:1-93.
10. Senkov M, Miracle W. Accelerated exploration of multi-principal element alloys with solid solution phases. Nat Commun. 2015;6(1):1-10.
11. Gorsse S, Couzinié J-P, Miracle DB. From high-entropy alloys to complex concentrated alloys. C R Phys. 2018;19(8):721-36.
12. Wang YP, Li DY, Parent L, Tian H. Improving the wear resistance of white cast iron using a new concept – High-entropy microstructure. Wear. 2011;271(9–10):1623-8.
13. Wang YP, Li DY, Parent L, Tian H. Performances of hybrid high-entropy high-Cr cast irons during sliding wear and air-jet solid-particle erosion. Wear. 2013;301(1-2):390-7.
14. Matsubara Y, Sasaguri N, Shimizu K, Yu SK. Solidification and abrasion wear of white cast irons alloyed with 20% carbide forming elements. Wear. 2001 Oct;250(1-12):502-10.
15. Purba RH, Shimizu K, Kusumoto K, Gaqi Y. Comparison of three-body abrasion behaviors of high-Cr-Mo- and High-Cr-Based multi-component white cast irons. J Mater Eng Perform. 2022
16. Pasini WM, Bellé MR, Pereira L, Amaral RF, Barcellos VK. Analysis of carbides in multi-component cast iron design based on high entropy alloys concepts. Mater Res. 2021;24(2):e20200398. http://dx.doi.org/10.1590/1980-5373-MR-2020-0398.
17. Bedolla-Jacuinde A, Guerra FV, Mejía I, Zuno-Silva J, Rainforth M. Abrasive wear of V–Nb–Ti alloyed high-chromium white irons. Wear. 2015;332-333:1006-11.
18. ASTM: American Society for Testing and Materials. ASTM G 133-05 (2016): standard test method for linearly reciprocating ball-on-flat sliding wear. West Conshohocken: ASTM International; 2016.
19. ASTM: American Society for Testing and Materials. ASTM D7755-11 (2022): standard practice for determining the wear volume on standard test pieces used by high-frequency, linear-oscillation (SRV) test machine. West Conshohocken: ASTM International; 2022.
20. Stefanescu DM. Thermal analysis: theory and applications in metalcasting. Int J Met Cast. 2015;9(1):7-22.
21. Thorpe WR, Chicco B. The Fe-rich corner of the metastable C-Cr-Fe liquidus surface. Metall Trans, A, Phys Metall Mater Sci. 1985;16(9):1541-9.
22. Hashimoto M, Nishiyama Y, Kaoru Y, Sasaguri N, Matsubara Y. Effects of carbon and molybdenum on mechanical and hot wear properties of multi-component white cast irons for steel rolling mill roll. Chuzo Kogaku. 2007;79(11):650-5.
23. Hashimoto M, Sasaguri N, Matsubara Y. Effects of carbon and nickel on mechanical and hot wear properties of multi-component white cast irons for steel rolling mill roll. Chuzo Kogaku. 2014;86(7):531-7.
24. Hashimoto M, Nishiyama Y, Sasaguri N, Matsubara Y. Influence of carbon and chromium on mechanical and hot wear properties of multi-component white cast irons for steel rolling mill rolls. Chuzo Kogaku. 2007;79(1):23-9.
25. Hashimoto M, Nishiyama Y, Sasaguri N, Matsubara Y. Influence of carbon and vanadium on mechanical and hot wear properties of multi-component white cast irons for steel rolling mill rolls. Chuzo Kogaku. 2006;78(5):238-44.